



Design and implementation of a ball-driven omnidirectional spherical robot



Wei-Hsi Chen, Ching-Pei Chen, Jia-Shiuan Tsai, Jackie Yang, Pei-Chun Lin *

Department of Mechanical Engineering, National Taiwan University, Taiwan

ARTICLE INFO

Article history:

Received 1 December 2011

Received in revised form 13 April 2013

Accepted 16 April 2013

Available online 20 May 2013

Keywords:

Spherical robot

Omnidirectional

Locomotion

ABSTRACT

We designed and implemented a novel omnidirectional spherical robot. Instead of using wheels or flywheels, a driven ball is installed inside the spherical shell and driven by two orthogonally-mounted rollers; thus, the omnidirectional mobility of the robot with no singularity can be achieved by simple forward kinematic mapping. The dynamic model of the robot is derived, and effect of the model's parameters is evaluated in simulation and discussed. The simulation results also serve as the design guideline for building the empirical system. Several design issues are addressed to ensure the robot's proper development. Finally, the spherical robot is built, and its performance is quantitatively and experimentally evaluated, thus proving its omnidirectional and trajectory-controllable mobility.

© 2013 Elsevier Ltd. All rights reserved.

1. Introduction

A spherical robot is a special type of mobile robot that has recently received significant attention. The special morphology of the robot has several advantages over a traditional wheeled or legged robot [1]: (i) the completely-covered outer shell protects the whole system; (ii) the motion resembles wheeled locomotion with great power efficiency and motion smoothness; (iii) the motion can be omnidirectional, owing to its intrinsic nature of geometrical symmetry; (iv) every portion of the outer shell can act as a “foot,” which allows fast collision recovery and automatic contact adapting to soft/uneven terrains and other conditions.

Several spherical robots have been reported in the past two decades, and they can be divided into three categories according to their driving mechanisms: direct-driving, gravity, and angular momentum methods. In the direct-driving method, with the design of a specific mechanism, the motor torque can be directly transmitted to the outer shell as the driving force for the robot. The concept was introduced in 1996 by Halme et al., where the robot had one active wheel mounted on the inside drive unit (IDU) with two points anchored to the outer shell [2]. The wheel can be steered so the robot can generate planar motion. The design was later revised by Zhan et al. in 2011; the weight of the robot was lightened and the number of anchors between the IDU and the outer shell was raised to four, and three were passive sponge wheels to improve the friction needed for robot steering [3]. In 1997, Bicchi et al. introduced the robot “SPHERICLE,” where a small wheeled vehicle was placed within the outer shell [4]. Later in 2003, Alves et al. proposed a robot with a similar driving mechanism. The robot had a four-wheeled car inside the shell, and through the independent control of these wheels, the robot could move forward and turn aside [5]. In 2002, Michaud et al. introduced the robot “Roball” with a novel driving system. The robot had two active wheels to form the IDU, and the contact points of these two wheels to the outer shell could be actively altered by changing the orientation of a heavy mass hanging on the IDU, thus achieving the driving and steering functions [6]. Many researchers were inspired by this “gimbal mechanism-like” design, and this later became one of the mainstream design approaches for spherical robots. In 2004, Kabała et al. introduced “RoBall,” the first spherical robot with an internal gimbal mechanism [7]. In 2006, Ming et al. reported a new configuration of a robot, which revised the gimbal mechanism by having a circular track around the shell's inner surface for the IDU to slide on [8]. In

* Corresponding author at: No. 1 Roosevelt Rd. Sec. 4, ME Eng. Bldg. Room 503-3, Taipei 106, Taiwan. Tel.: +886 2 3366 9747; fax: +886 2 2363 1755.
E-mail address: peichunlin@ntu.edu.tw (P.-C. Lin).

2008, a gimbal-based spherical robot “BYQ-III” was introduced by Liu et al. and a series of comprehensive studies on the control and trajectory planning of this robot was reported as well [9–11]. Some other robots with similar mechanisms were also reported by Ghanbari et al. [12], Yoon et al. [13], and others.

The second category is the gravity method. By manipulating the center of mass (COM) position of the robot, a torque can be adequately created with respect to the ground contact point, thus driving the robot to roll. In 1999, Mukherjee et al. introduced a novel configuration of a spherical robot “Spherobot,” which had four movable masses mounted on the four spokes extending from its geometrical center to the shell. When the masses moved along with the spokes, which altered the COM of the whole robot, the robot could be driven in a desired direction [14]. The concept was further analyzed by Javadi in 2002; the robot “Glory” could radically distribute weights along with the spokes, which enabled the robot to accelerate, decelerate, and move at a constant velocity [15,16].

The third category is the angular momentum method, which utilizes the characteristics of angular momentum conservation. When a flywheel installed inside the spherical robot rotates, the outer shell rotates in the opposite direction to balance the angular momentum. In 2000, Bhattacharya et al. reported a robot design in this category. It had two sets of orthogonally-mounted motors attaching to the spherical shell, and the shell rotated in the opposite direction as the motor rotated. With their axes parallel and perpendicular to the ground, these motors are for driving and steering, respectively [17]. Following that, a series of studies on this type of robot was reported by Joshi et al. [18,19]. In 2009, Jia et al. reported a spherical robot with only one orientation-changeable flywheel, achieving both driving and steering [20]. While driving and steering are two independent degrees of freedom (DOFs), they may be generated by different methods. In 2008, Schroll introduced a “Gyrosphere robot,” which combined the angular momentum (for driving) and gravity (for steering) methods [21].

Each method has its advantages and disadvantages, and the discussion here focuses on mobility. Considering the driving characteristics, the direct-driving method directly transmits the motor torques to the robot’s outer shells. Thus, comparable to the gravity method, the propulsion force is controllable. In addition, that force can be extended to a larger scale that is feasible for fast locomotion and obstacle negotiation. The angular momentum method can excite a great propulsion force. However, since the momentum balance is in the velocity state, empirically, the motion is hard to control in displacement, thus posing a challenge in robot trajectory planning. Considering the steering capability, one of the most important characteristics is the omnidirectional mobility since it is a unique feature of the spherical robots, as described in the first paragraph. Omnidirectional mobility by definition indicates that the robot can move in any direction at any instant, or equivalently, having controllable motion DOFs as the coordinate system. The planar coordinate system in general has three DOFs: forward/backward motion, lateral motion, and orientation. However, since the spherical robot is symmetric in orientation, the omnidirectional locomotion in spherical robots means they can move freely in the forward/backward and lateral directions, reducing to two DOFs. Robots using the gravity method can move omnidirectionally, but their trajectory planning is challenging since the motion is determined by the spatial composition of the continuously-rotating active inputs, whose number is usually larger than two DOFs. Robots with one flywheel (i.e., angular momentum method) are not able to perform omnidirectional locomotion since the direction of the angular momentum changes gradually, resulting in a gradual change of their direction. In contrast, robots with two flywheels can perform omnidirectional motion in most situations. However, because the flywheels are anchored to the outer shell at certain positions, such robots have certain singular configurations, which limit their movement to a certain direction. The similar situation of singularity occurs in robots with the gimbal-mechanism-based direct-driving method. Robots with the friction-based direct-driving method do not have a singularity problem. However, the developed robots which utilize wheels have nonholonomic constraints, so they cannot perform instant sharp turns (i.e., not omnidirectional). The characteristics of the robots with different configurations are summarized in Fig. 1. The index “sharp turn” indicates that the robot is capable of performing sharp turn motions “at any position.” For example, a robot with a single wheel can perform a sharp turn by changing the wheel’s orientation. However, this change requires a certain amount of time, so the locomotion does not qualify as

Robot Configuration		Single wheel	Hamster car	Pendulum on rotating axis	Gimbal mechanism	Single ball	Mass movement	Orthogonally mounted flywheels	Flywheel on pendulum	Parallelly mounted flywheels
Driving mechanism	Driving	D	D	D		D	G	A	D/A	A
	Steering	D	D	D		D	G	A	A	G
Input needed		2	≥ 2	2		2	4	2	3	2
Sharp turn		V	V	V*		V	V	V*	V	
Omnidirectional locomotion				V*		V	V	V*		

Fig. 1. Characteristics of the developed spherical robots. D, G, and A indicate direct-driving, gravity, and angular momentum methods, respectively. The mark “V” indicates the robot is capable of performing the specific motion, and the mark “V*” indicates the motion is achievable in most situations (i.e., with singularity).

omnidirectional. In other words, the omnidirectional motion can be regarded as the capability of performing sharp turn motions "at any instant."

Here, with the desire to develop a spherical robot capable of omnidirectional locomotion and trajectory control, yet with a minimum number of actuators, we report on a novel design of a spherical robot *OmniQiu*. The robot utilizes the direct-driving method. However, instead of wheels or the gimbal-mechanism adopted by other robots in this category, a smaller ball is installed inside the shell and can be driven to roll on the shell by two independent and orthogonally-mounted actuators, thus achieving 2-DOF singularity-free planar omnidirectional locomotion of the spherical robot. To the best of our knowledge, this unique configuration of the spherical robot has never been reported. The relation from actuators to the robot locomotion is 2 to 2 mapping with simple functions, thus achieving the requirement of using minimum actuators and requiring low control effort.

The paper is organized as follows. The design concept of the spherical robot *OmniQiu* is introduced in Section 2, and the derivation of its dynamic model based on Lagrangian mechanics is described in Section 3. The design realization is presented in Section 4, and the performance evaluation is reported in Section 5. Section 6 concludes the work.

2. Design concept

Design of the spherical robot is set to meet the following specifications: (i) The robot uses the direct-driving method, which utilizes the motor power to directly drive the spherical robot via the transmission system. (ii) It is capable of performing omnidirectional locomotion. As mentioned in the Introduction, omnidirectional locomotion by definition indicates that the robot can move in "any" direction at every instant. For a spherical robot, the mobility in 2-DOF planar translational motion (i.e., forward/backward and sideways) is required. (iii) It uses minimum number of actuators to achieve desired motion. Since the omnidirectional motion of the spherical robot is 2 DOF, two motors are utilized.

Design of the spherical robot with singularity-free omnidirectional locomotion using the direct-driving method requires the mechanism inside the robot to have non-fixed contact points to the outer shell to execute continuous rolling motion of the shell. Thus, the most widely-used method to satisfy this is to install one or multiwheels inside the spherical shell. However, the fixed standard wheel ideally prevents the motion orthogonal to the rolling direction [22], thus impeding omnidirectional locomotion. We focused our attention on the mechanism design of the traditional ball mouse, which has a freely-rolling track ball and two orthogonally-oriented rotating rollers next to the ball. As the track ball rotates, its rolling motion can be decomposed into two directions, each driving one roller only, so the planar motion of the ball can be correctly measured. Inspired by this unique arrangement, we design the spherical robot *OmniQiu* by the mechanism "inversed" to that in the ball mouse—by actively and independently driving two rollers, the motion of the track ball can be composed to successfully roll in any direction on the plane. Following that, by putting the track ball and the whole driving system inside the spherical shell, the spherical robot can be conceptually constructed. The planar rolling of the track ball drives the spherical shell moving freely on the 2D plane; thus the omnidirectional motion of the spherical robot is achieved.

Fig. 2 sketches the driving mechanism of the proposed spherical robot from the front view (A) and the top view (B). As shown in Fig. 2(A), when the y-axis roller rotates in the clockwise direction (i.e., viewed from +y direction) with speed $\dot{\theta}_r$, the track ball can be driven to roll in the counterclockwise direction inside the spherical shell with speed $\dot{\theta}_d$, which further drives the shell to roll in the same counterclockwise direction on the ground with speed $\dot{\theta}_s$. As a result, the spherical robot moves toward +x direction. In the meantime, because the x-axis roller contacts the driven ball via a single point located in its great circle as shown in Fig. 2(B), the rolling motion generated by the y-axis roller is not affected by this contact point. Thus, the planar motion of the driven ball can be independently controlled and actuated by two rollers, which eases the motion planning and trajectory generation. Since the function of the "track ball" is no longer tracking, that ball is hereafter referred to as the "driven ball." To maintain the relative configuration among the spherical shell, the driven ball, and the two rollers, a structure is constructed to define the allowable relative motion among these parts. In addition, the structure is also utilized as the fixture to the required mechatronic system. As a result, the structure and the mechatronics are all installed inside the outer shell in the remaining space, as encircled in the dash-dotted curve shown in Fig. 2(A). These parts, including two rollers, are hereafter referred to as the "main

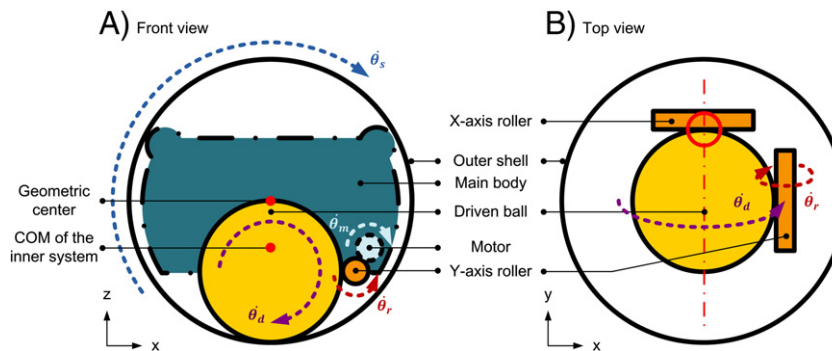


Fig. 2. Illustrative sketches of the spherical robot's driving system: (A) front view and (B) top view. The main body and the motors are not drawn in (B) for clear presentation.

body." With adequate contact between the main body and the outer shell, the driving mechanism can be established and the driven ball can be adequately driven by the two rollers. The combined system with the main body and the driven ball is hereafter referred to as the "inner system."

The empirical configuration of the inner system is constrained by its desired COM with respect to the spherical robot's geometric center (i.e., also the COM of the outer shell). If the COM coincides with the geometric center, the inner system is in neutral equilibrium, and the contact point between the driven ball and the outer shell may exist at any point. If the COM of the inner system is located above the robot's geometric center, the system acts like an inverted pendulum, and the stable configuration of the inner system will be an inverted version of the configuration shown in Fig. 2(A). In this condition, there is less contact friction between the outer shell and the driven ball than the ordinary configuration since the gravity vector aims in the opposite direction than the normal force. As a result, the COM of the inner system located below the spherical robot's geometric center is desired.

The DOFs of the robot shown in Fig. 2 may be interpreted as having different numbers, depending on the subsystems to be judged. Considering the robot's explicit behavior (i.e., the motion of the outer shell), it only has two translational and planar DOFs since the rotational DOF does not alter its appearance. Considering the state of the main body presented at the outer shell's geometric center, the robot has five DOFs, including the two translational DOFs described above and three rotational DOFs in spatial space, where the last DOF, vertical displacement, does not change during locomotion. The designed control input has two DOFs (i.e., rotation of the two rollers), which matches the DOFs of the robot's explicit behavior as planned. Because of Newton's third law, when the torque applies to the roller to roll the driven ball, the reaction torque applies to the main body simultaneously and makes it rotate. Thus, each control input indeed affects two DOFs of the main body—one translational DOF and one rotational DOF. Two control inputs determine four out of five DOFs of the main body. The left yaw DOF of the main body (i.e., rotation about the vertical axis) cannot be controlled by the roller inputs. However, generally, only the explicit behavior matters and this rotation does not change the robot's explicit appearance. In addition, the explicit motion variation caused by the variation of this DOF can be corrected with control effort by adjusting the relative motion of these two controlled inputs.

3. Robot dynamic model

The dynamic model of the spherical robot as it rolls along in a straight line (i.e., in +x direction) is developed in this section according to the Lagrangian method. Because the driving mechanism of the robot for movement along x and y directions are identical, as shown in Fig. 2, the simplified planar model in the xz-plane is developed and depicted in Fig. 3. Note that the planar model is also suitable for not only the "driven ball" in spherical shape, but also for the ordinary wheels in the thin disk shape. Thus, the model development can be utilized in a much wider class of devices as shown in Fig. 1.

The model is composed of three parts: the outer shell (in brown), the driven ball (in blue), and the main body (in green), which matches the composition of the designed system described in Section 2. The three parts are assumed to be axis-symmetric, so their COMs can be aligned to position in a straight line. In addition, all contacts are assumed to engage in pure rolling without slipping. Thus, the rotational motion of the driven ball, θ_d , shown in Fig. 2(A) is directly related to that of the roller, θ_r , so modeling of the roller does not attribute extra dynamic property and can be skipped. The torque generated from the motor and applied to the roller can directly be regarded as applying to the driven ball by scaling the ratio of two radii. Because the motor rotates with respect to its housing (i.e., the main body), θ_d is a relative angle with respect to the main body. In contrast, the rotational motion of the outer shell, θ_s , is defined with respect to the ground. The swing motion of the main body represented by the rotational state θ_b , is also defined with respect to the vertical z-axis. The complete nomenclature of the modeling work is listed in Table 1.

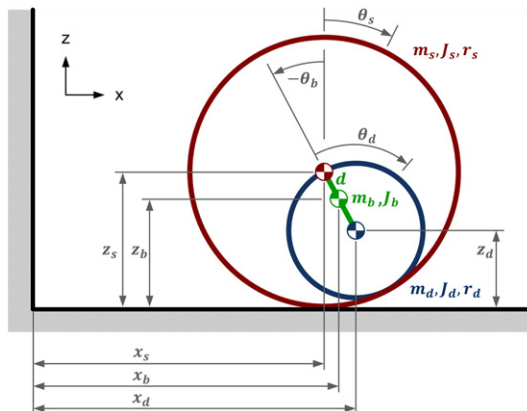


Fig. 3. Parameters of the robot dynamic model. Related definitions are listed in Table 1.

Table 1

Nomenclature of the model and the corresponding robot specifications.

Outer shell		
Radius	r_s	121.5 mm
Mass	m_s	360 g
Moment of inertia	J_s	$3.3 \times 10^6 \text{ g} \cdot \text{mm}^2$
COM position vector	(x_s, z_s)	
Orientation	θ_s	
Driven ball		
Radius	r_d	60 mm
Mass	m_d	100 g
Moment of inertia	J_d	$0.2 \times 10^6 \text{ g} \cdot \text{mm}^2$
COM position vector	(x_d, z_d)	
Orientation	θ_d	
Main body		
Mass	m_b	1140 g
Moment of inertia	J_b	$4.4 \times 10^6 \text{ g} \cdot \text{mm}^2$
COM position vector	(x_b, z_b)	
Orientation	θ_b	
Driving mechanism		
Roller radius	r_r	5 mm
Roller rotation	θ_r	
Distance between the COMs of the outer shell and of the main body	d	10 mm
Coefficients	A	$6.4 \times 10^6 \text{ g} \cdot \text{mm}^2$
	B	$1.2 \times 10^7 \text{ g} \cdot \text{mm}^2$
	C	16550 g · mm
	D	$3.0 \times 10^7 \text{ g} \cdot \text{mm}^2$
Gear ratio	n_p	64
	n_r	12

The translational (K_1) and rotational (K_2) kinetic energy as well as the potential energy (U) of the whole system can be expressed as:

$$\begin{cases} K_1 = \frac{1}{2} m_s (\dot{x}_s^2 + \dot{z}_s^2) + \frac{1}{2} m_b (\dot{x}_b^2 + \dot{z}_b^2) + \frac{1}{2} m_d (\dot{x}_d^2 + \dot{z}_d^2) \\ K_2 = \frac{1}{2} J_s \dot{\theta}_s^2 + \frac{1}{2} J_b \dot{\theta}_b^2 + \frac{1}{2} J_d (\dot{\theta}_d + \dot{\theta}_b)^2 \\ U = m_s g z_s + m_b g z_b + m_d g z_d \end{cases}. \quad (1)$$

Since non-slip rolling is assumed, the position vectors of the outer shell, the main body, and the driven ball can be further written as:

$$\begin{cases} (x_s, z_s) = r_s \theta_s, r_s \\ (x_b, z_b) = (r_s \theta_s - d \sin \theta_b, r_s - d \cos \theta_b) \\ (x_d, z_d) = (r_s \theta_s - (r_s - r_d) \sin \theta_b, r_s - (r_s - r_d) \cos \theta_b) \end{cases} \quad (2)$$

respectively, with a constraint equation that describes the relationships among θ_s , θ_b , and θ_d :

$$f(\theta_s, \theta_b, \theta_d) = r_s(\theta_s - \theta_b) - r_d \theta_d = 0. \quad (3)$$

The states θ_d and θ_b are chosen as the general coordinates, which are directly affected by the motor torque (i.e., action and reaction torques). By importing Eq. (3) into Eqs. (1) and (2), the total kinetic energy K and the potential function U can be derived:

$$\begin{aligned} K = K_1 + K_2 &= \frac{1}{2} \left[(m_s + m_d + m_b) r_d^2 + \left(\frac{r_d}{r_s} \right)^2 J_s + J_d \right] \dot{\theta}_d^2 \\ &\quad + \frac{1}{2} \left[(m_s + m_d + m_b) r_s^2 + m_b d^2 + m_d (r_s - r_d)^2 - 2(m_b d + m_d(r_s - r_d)) r_s \cos \theta_b + J_s + J_b + J_d \right] \dot{\theta}_b^2 \\ &\quad - \left[(m_s + m_d + m_b) r_s r_d - (m_b d + m_d(r_s - r_d)) r_d \cos \theta_b + \frac{r_d}{r_s} J_s + J_d \right] \dot{\theta}_s \dot{\theta}_b \end{aligned} \quad (4)$$

$$U = m_s g r_s + m_b g (r_s - d \cos \theta_b) + m_d g (r_s - (r_s - r_d) \cos \theta_b). \quad (5)$$

Importing energy terms in Eq. (4) into the Lagrangian equation,

$$\tau = \frac{d}{dt} \frac{\partial K}{\partial \dot{\theta}} - \frac{\partial K}{\partial \theta} + \frac{\partial U}{\partial \theta}, \quad (6)$$

yields

$$\begin{aligned}\tau_d = & \left[(m_s + m_b + m_d)r_d^2 + \left(\frac{r_d}{r_s}\right)^2 J_s + J_d \right] \ddot{\theta}_d \\ & + \left[(m_s + m_b + m_d)r_s r_d - (m_b d + m_d(r_s - r_d))r_d \cos \theta_b + \frac{r_d}{r_s} J_s + J_d \right] \ddot{\theta}_b \\ & + [m_b d + m_d(r_s - r_d)]r_d \dot{\theta}_b^2 \sin \theta_b\end{aligned}\quad (7)$$

and

$$\begin{aligned}\tau_b = & \left[(m_s + m_b + m_d)r_s r_d - (m_b d + m_d(r_s - r_d))r_d \cos \theta_b + \frac{r_d}{r_s} J_s + J_d \right] \ddot{\theta}_d \\ & + \left[(m_s + m_b + m_d)r_s^2 + m_b d^2 + m_d(r_s - r_d)^2 - 2(m_b d + m_d(r_s - r_d))r_s \cos \theta_b \right. \\ & \left. + J_s + J_b + J_d \right] \ddot{\theta}_b + \left[m_b d + m_d(r_s - r_d) \right] r_s \dot{\theta}_b^2 \sin \theta_b \\ & + [m_b d + m_d(r_s - r_d)]g \sin \theta_b.\end{aligned}\quad (8)$$

Note that τ_d and τ_b are torques acting on the driven ball and the main body, respectively, and they are generated by the motor torque. As shown in Fig. 2(A), when the motor generates a torque τ_m , the main body where the motor is mounted feels a reaction torque $\tau_b = -\tau_m$. The torque τ_m applied to the roller is further transmitted to the driven ball. Because these two parts have different radii, the torque acting on the driven ball is magnified to $\tau_d = n_r \tau_m$, where n_r is the ratio of radius of the driven ball to that of the roller. By rearranging Eqs. (7) and (8), $\ddot{\theta}_d$ and $\ddot{\theta}_b$ can be represented as:

$$\ddot{\theta}_d = -\frac{1}{r_m A(D-2Cr_s \cos \theta_b)-(B-Cr_d \cos \theta_b)^2} \tau_m + \frac{\left[(B-Cr_d \cos \theta_b)g + (Br_s - Dr_d + Cr_s r_d \cos \theta_b)\dot{\theta}_b^2 \right] C \sin \theta_b}{A(D-2Cr_s \cos \theta_b)-(B-Cr_d \cos \theta_b)^2} \quad (9)$$

$$\ddot{\theta}_b = \frac{1}{r_m A(D-2Cr_s \cos \theta_b)-(B-Cr_d \cos \theta_b)^2} \tau_m - \frac{\left[Ag + (Ar_s - Br_d + Cr_d^2 \cos \theta_b)\dot{\theta}_b^2 \right] C \sin \theta_b}{A(D-2Cr_s \cos \theta_b)-(B-Cr_d \cos \theta_b)^2} \quad (10)$$

and $\ddot{\theta}_s$ can be derived by Eqs. (3), (9), and (10):

$$\ddot{\theta}_s = -\frac{1}{r_s r_m} \frac{Dr_d^2 + Ar_s r_m - B(r_s + r_m)r_d - C(r_s - r_m)r_d^2 \cos \theta_b}{A(D-2Cr_s \cos \theta_b)-(B-Cr_d \cos \theta_b)^2} \tau_m - \frac{1}{r_s} \frac{\left[(Ar_s - Br_d + Cr_d^2 \cos \theta_b)g + (Ar_s^2 - 2Br_s r_d + Dr_d^2)\dot{\theta}_b^2 \right] C \sin \theta_b}{A(D-2Cr_s \cos \theta_b)-(B-Cr_d \cos \theta_b)^2} \quad (11)$$

and $A = \left[(m_s + m_d + m_b)r_d^2 + \left(\frac{r_d}{r_s}\right)^2 J_s + J_d \right]$, $B = \left[(m_s + m_d + m_b)r_s r_d + \frac{r_d}{r_s} J_s + J_d \right]$, $C = [m_d(r_s - r_d) + m_b d]$, and $D = [(m_s + m_b + m_d)r_s^2 + m_b d^2 + m_d(r_s - r_d)^2 + J_s + J_b + J_d]$ are mainly inertia parameters of various parts of the robot.

Eqs. (10) and (11) show that dynamic responses of the main body and outer shell, $\ddot{\theta}_b$ and $\ddot{\theta}_s \ddot{\theta}_s$, are functions of θ_b , $\dot{\theta}_b$, and the motor torque, τ_m . These relationships can be symbolically represented as $\ddot{\theta}_b = f(\theta_b, \dot{\theta}_b, \tau_m)$ and $\ddot{\theta}_s = f(\theta_b, \dot{\theta}_b, \tau_m)$. Thus, the spherical robot's dynamic performance is mainly affected by the state of the main body and the torque. More specifically, the coefficients in front of τ_m can be treated as the inverse of the equivalent inertia, so this term relates the robot's input torque and output angular acceleration. The second term on the right side of Eqs. (10) and (11) can be treated as the equivalent gravity and centrifugal effect resulting from the main body's dynamics, so this term alters the robot's effective torque and only exists when the main body is tilted.

The behavior of the DC brushed motor with a planetary gearbox and with a constant voltage input, v , can be approximated by an affine function:

$$\tau_m = \eta n_p \left(\frac{K_T v}{R} - \frac{K_T K_e}{R} n_p \dot{\theta}_m \right), \quad (12)$$

where K_T , K_e , R , n_p , and η are the torque constant, the voltage constant, the terminal resistance, the gear ratio of the gearbox, and the gearbox efficiency, respectively. By importing Eqs. (12) into (10) and (11), the overall dynamic relationship of the control input to the robot output is established.

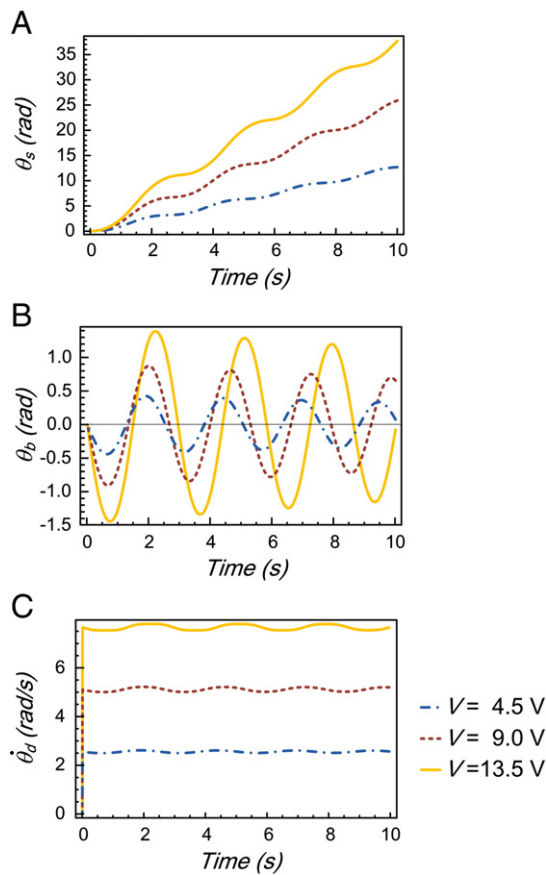


Fig. 4. Simulation results that show the effect of the input voltage on the system's dynamics: (A) rotation of the outer shell, θ_s ; (B) orientation of the main body, θ_b ; and (C) speed of the driven ball, $\dot{\theta}_d$. The input voltages are 4.5 V (dash-dotted blue), 9 V (dashed red), and 13.5 V (solid yellow).

The effect of the input and parameters on the overall system's dynamics can be revealed through the numerical simulation of the model described above. The variables for evaluation include the input voltage to the motor, the masses, and the COM position of the main body. The system's dynamics are evaluated by the body state of the outer shell, the driven ball, and the main body. Each variable is adjusted for three different values in simulation to check its effect on the system's dynamics. The middle value is chosen according to the one used in the empirical system, which is listed in Table 1. The larger and smaller values are chosen to be 50% more and 50% less, respectively. Fig. 4 plots the effect of the input voltage on the system's dynamics. Fig. 4(A) reveals that the speed of the robot (i.e., explicit behavior, $\dot{\theta}_s$) is faster with higher input voltage, yet small oscillations of θ_s during motion are observed in all simulated input voltages. This phenomenon mainly results from the oscillating behavior of the main body shown in Fig. 4(B). It shows that the oscillating frequency of θ_b remains similar among different input voltages, but the amplitude of θ_b is roughly proportional to the input voltage. The main body inside the outer shell can be treated as the pendulum system. When the geometry and mass are fixed to certain values, the system has its own natural frequency. Thus, a change in the input voltage has less effect on the frequency of θ_b but more on the amplitude since the torque generated by the input voltage and applied to the system on some level disturbs the system's equilibrium. Larger torque yields larger perturbation. Fig. 4(C) shows that the driven ball reaches its steady-state speed in a short amount of time, but it also has small oscillations due to the main body's swinging and the system's dynamics. Because three body states, $\dot{\theta}_s$, $\dot{\theta}_d$, and $\dot{\theta}_b$, are constrained by Eq. (3), the robot's explicit behavior, $\dot{\theta}_s$, includes oscillations. In brief, this simulation indicates that the voltage is important for the robot's forward speed, and the behavior of θ_b is important for its detailed explicit behavior.

Fig. 5 plots the effect of the input voltage on the system's dynamics. Fig. 5(A-I, II, III) shows that variations in the mass do not alter the explicit forward speed of the robot $\dot{\theta}_s$ much, regardless of whether the variations of mass involve the driven ball, the outer shell, or the main body. In contrast, because of the “pendulum behavior” described in the previous paragraph, variations indeed have a significant effect on the oscillating behavior of θ_b . As shown in Fig. 5(B-I, II), when the mass of the main body or the driven ball increases, the oscillating frequency of the main body increases and its amplitude decreases. This phenomenon matches the behavior of the pendulum. In contrast, because the outer shell acts as the base for oscillation, a heavier mass has the opposite effect, as shown in Fig. 5(B-III). Fig. 5(C-I, II, III) reveals that the transient response and the steady-state condition of the driven

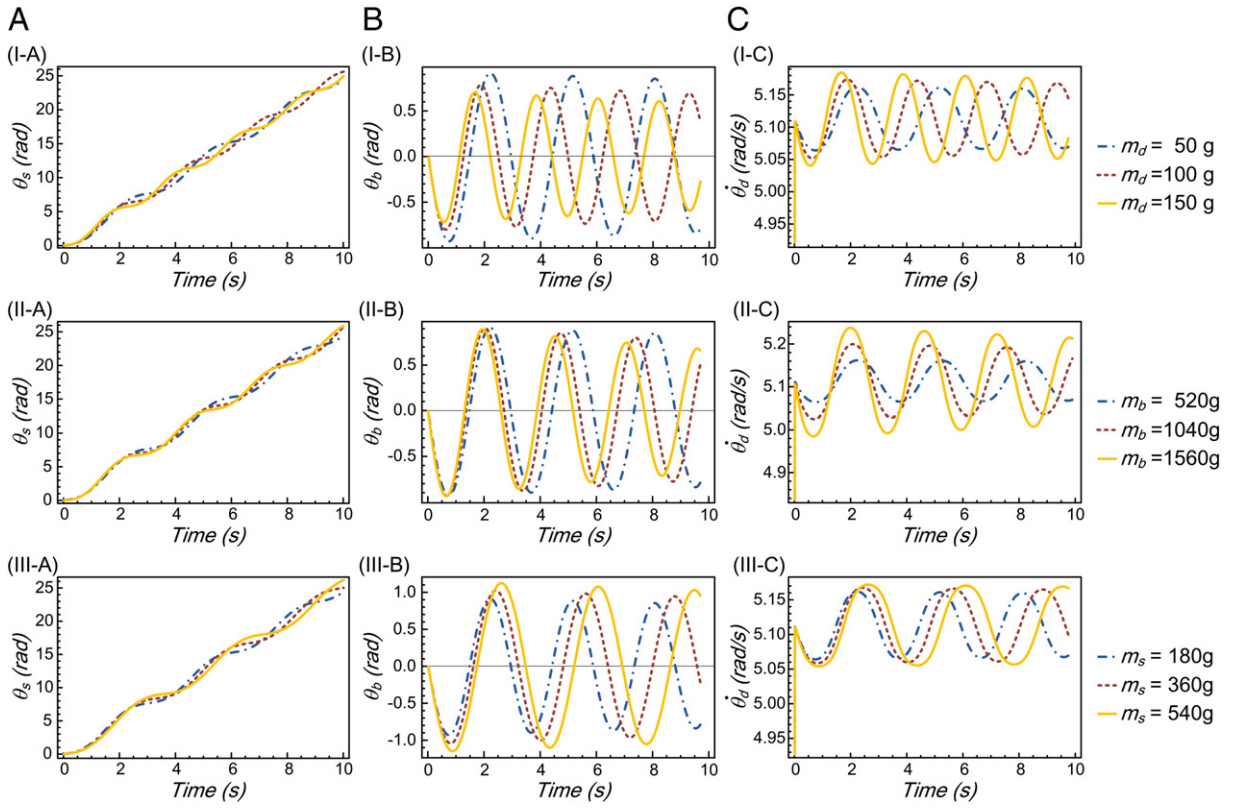


Fig. 5. Simulation results that show the effect of the mass of the driven ball, the main body, or the outer shell on the system's dynamics: (A) rotation of the outer shell, θ_s ; (B) orientation of the main body, θ_b ; and (C) speed of the driven ball, $\dot{\theta}_d$. The mass variations are executed on the driven ball (I), the main body (II), and the outer shell (III), respectively. The dash-dotted blue, dashed red, and solid yellow lines represent the lighter mass (50% less), the nominal mass, and the heavier mass (50% more), respectively.

ball do not significantly change when the mass varies. The driven ball oscillates and reaches its final angular velocity within a short amount of time. In brief, this simulation confirms that the mass of the main body has significant effect on its oscillating behavior.

Fig. 6 plots the effect of the COM position of the main body on the system's dynamics. The COM position is characterized by the parameter d shown in Fig. 3. Similar to the results shown in Fig. 5, variations in the position do not significantly alter the explicit forward speed of the robot $\dot{\theta}_s$, as shown in Fig. 6(A). However, they have a significant effect on the oscillating behavior of θ_b because of its “pendulum behavior,” as shown in Fig. 6(B). When the parameter d increases, the oscillating frequency of the main body also increases, and its amplitude decreases. Similarly, Fig. 6(C) reveals that the transient response and the steady-state condition of the driven ball do not significantly change when d varies. Note that in the empirical implementation, the space for parameter variation is limited. The input voltage is usually reserved for active control input, which is not a design parameter. The mass of the robot's components is usually set to be composed of lighter materials since this, in general, yields a larger power density of the system. Thus, the mass may not be a good parameter to be adjusted. As a result, the COM position of the main body may be regarded as the only active parameter that should be considered in the design period.

4. Design realization

Though the basic structure of *OmniQiu* only contains three subsystems (i.e., the outer shell, the driven ball, and the main body with two driving rollers), various issues make it challenging to apply the design to the empirical world, which are addressed in this section.

4.1. Driving system

As mentioned in Section 2, the driven ball is driven by two orthogonally mounted rollers at its largest circle and on the horizontal plane. With this design, the motions of the driven ball propelled by these two rollers are independent to each other, which ease the robot's overall motion control and trajectory planning. Owing to the tight space around the roller, a spur-gear

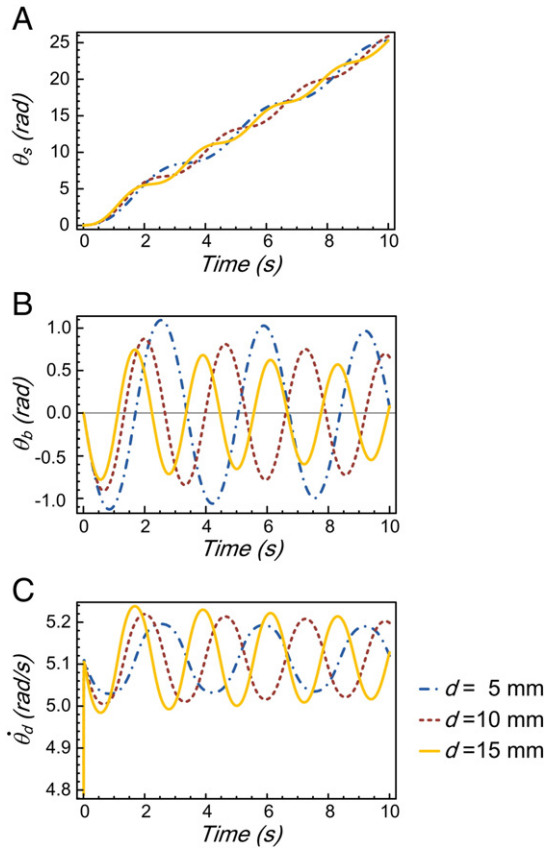


Fig. 6. Simulation results that show the effect of the COM position of the main body, d , on the system's dynamics: (A) rotation of the outer shell, θ_s ; (B) orientation of the main body, θ_b ; and (C) speed of the driven ball, $\dot{\theta}_d$. The d positions in the three subfigures are 5 (dash-dotted blue), 10 (dotted red), and 15 (solid yellow), respectively.

transmission (gear ratio 1:1) is utilized between the roller and the small DC motor (IG-12GM 01, Shayang Ye Co. Ltd.) with a planetary gearbox (gear ratio 64:1, $n_p = 64$). With the assumption of pure rolling (i.e., the same tangential velocity v_t at all rolling interfaces), the forward speed can be derived as:

$$v_t = \dot{\theta}_r r_r = \dot{\theta}_d r_d = \dot{\theta}_s r_s, \quad (13)$$

as shown in Fig. 2(A). In addition, the magnitude of the tangential velocity v_t is also equal to the forward speed of the robot. With a rated motor speed of 10,000 rpm, the forward velocity is calculated as 0.13 (m/s).

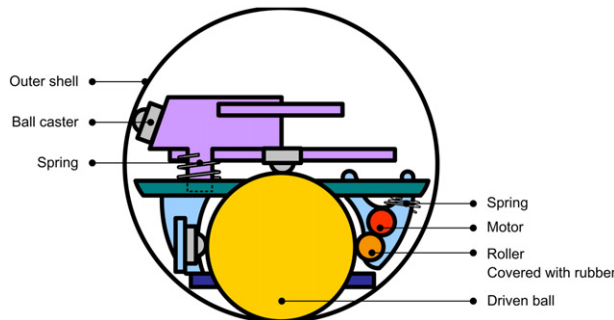


Fig. 7. The supporting system, pressure mechanisms, and the finished mechanism.

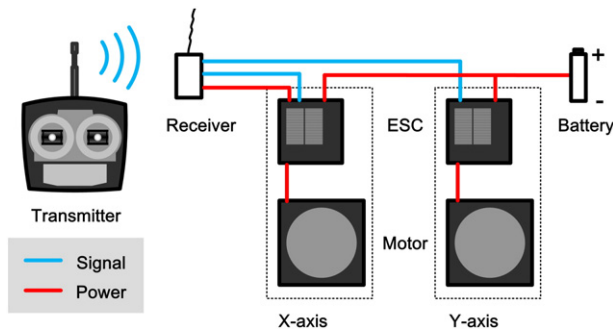


Fig. 8. Mechatronic system of the robot.

In the empirical system, since the two rollers in *OmniQiu* are mounted orthogonally to each other and both are in charge of the motion in a specific direction, the explicit planar motion of the robot on the ground can be generated by simple composition of the roller motions:

$$\begin{bmatrix} \dot{x} \\ \dot{y} \end{bmatrix} = \begin{bmatrix} \frac{1}{n_p} r_r & 0 \\ 0 & \frac{1}{n_p} r_r \end{bmatrix} \begin{bmatrix} \dot{\theta}_{m,x} \\ \dot{\theta}_{m,y} \end{bmatrix}. \quad (14)$$

The symbols $\dot{\theta}_{m,x}$ and $\dot{\theta}_{m,y}$ are the angular velocity of the motors, which drive y-axis roller and x-axis roller, respectively. The mapping function indicates the standard forward kinematics of the robot from inputs of the motor speeds to the output of the robot velocity. Owing to the orthogonality, the mapping is decoupled between these two inputs/outputs.

4.2 . Friction issue

Like other wheeled-based spherical robots described in the [Introduction](#), the robot *OmniQiu*'s motion generation requires adequate frictional forces acting between all rolling interfaces. In addition, pure rolling behavior is preferred for control purposes. Because the friction force is determined by the friction coefficient and the normal force, in the empirical implementation the design focuses on increasing both factors between the rolling surfaces. Several design features are implemented to strength the rolling behavior between the roller and the driven ball: (i) the roller is covered with a rubber tube, which has a high friction

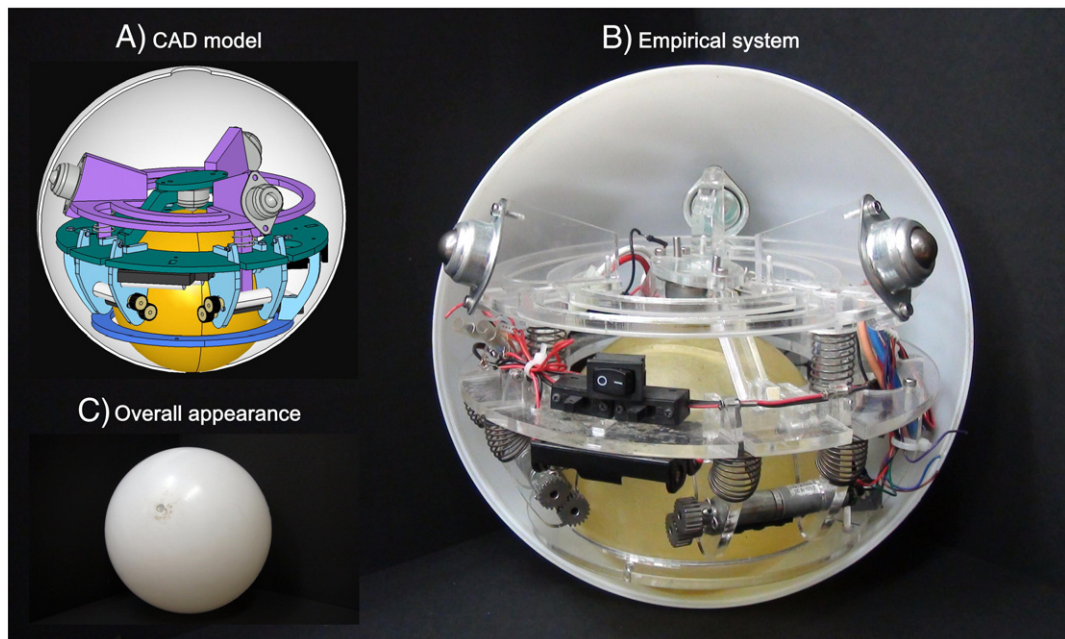


Fig. 9. The CAD model (A) and the images of the spherical robot *OmniQiu* (B and C).

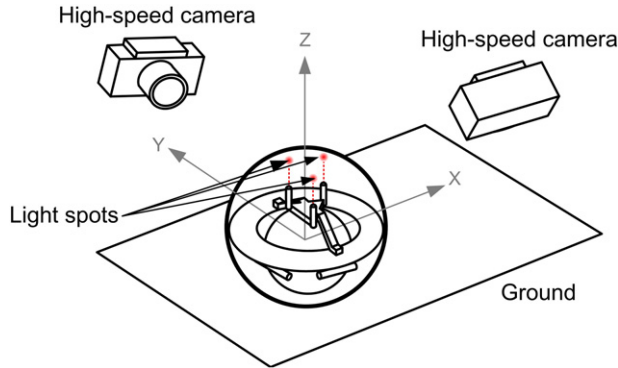


Fig. 10. Experimental setup for performance evaluation.

coefficient to the plastic surface of the driven ball. (ii) A spring mechanism is also installed to push the roller toward the driven ball, thus providing essential normal force and compensating for the imperfect driven ball's small shape variations. (iii) Two ball casters are installed on top of the driven ball and on the opposite side of the rollers, respectively, thus fixing the relative configuration of the driven ball to the main body as well as reducing the friction generated at these contact points. Three ball casters are installed between the main body and the outer shell to adequately attach the main body to the shell. The normal force between the driven ball and the outer shell can be expressed as

$$N_{ds} = N_{bs} + (m_b + m_d)g \cos \theta_b, \quad (15)$$

where N_{ds} and N_{bs} are the normal forces between the driven ball and the outer shell and between the main body and the outer shell, respectively. In order to provide enough friction force for rolling, N_{ds} should be sufficiently large and kept at a certain value while the contact condition varies. As a result, a spring mechanism is mounted between the ball caster and the main body to improve the rolling behavior between the driven ball and the outer shell. In addition to the spring forces, the weight of the main body and the driven ball could be utilized as the source of N_{ds} . However, this approach is not adopted here since the robot's dynamic response will be slower with increased weight, as described in Section 3. On the other hand, a small θ_b can result in a greater N_{ds} according to the second term of Eq. (15). The illustrative diagram of the mechanisms is depicted in Fig. 7.

4.3. Mechatronic system

Fig. 8 shows the mechatronic system of the *OmniQiu*. A RF-based transmitter/receiver pair (T2ER, Futaba) is utilized for the communication between the *OmniQiu* and the remote operator. The control signal sent from the operator can be well recognized by the receiver, and it is sent to an electric speed control (ESC, TAMIYA, TEU-101BK) that drives the motor with a pulse-width-modulation (PWM) method. Thus, the motor's speed can vary. The robot is operated on 9 V according to the specifications of the receiver, motor drivers, and the motors. Six nickel–metal hydride (NiMH) AA batteries are used as power source. Further, through the gear pair and the rolling mechanism, the robot can be driven according to remote commands. The robot's planar motion can be adequately generated through the composition of the rolling motions along with two rolling axes based on Eq. (14).

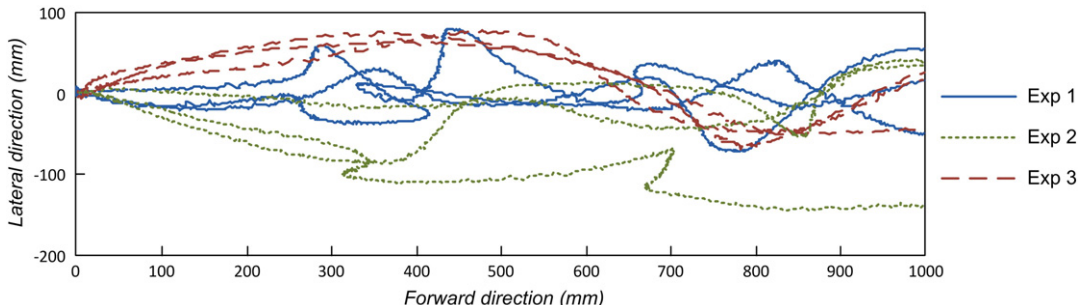


Fig. 11. The trajectories of the robot's geometrical center while it is driven by the x-axis roller (Exp 1), the y-axis roller (Exp 2), and two rollers simultaneously (Exp 3).

Table 2

Root mean squared error of the robot in the experiments.

	Lateral displacement (mm)	Yaw orientation (deg)
	Mean (std)	Mean (std)
Exp 1	26 (7.47)	5 (0.96)
Exp 2	56 (35.92)	10 (4.94)
Exp 3	41 (1.44)	13 (3.94)

5. Performance evaluation

Table 1 lists the overall specifications of the spherical robot *OmniQiu*. Fig. 9(A) depicts the complete CAD model of the system and Fig. 9(B) shows the picture of the empirical system. The outer shell's material was obtained from a company that manufactures globes. The structure of the main body was constructed with acrylic sheets owing to their easy manufacturability by a laser cutter. Because the configuration of the main body was not symmetrical with respect to the vertical axis owing to the installation of various components, the heavy-weight components such as batteries were carefully arranged for two purposes: (i) to balance the weight distribution of the main body so its COM could be aligned with the central line of the whole system; and (ii) to lower the COM of the main body, thus reducing its tilt phenomenon and improving the robot's dynamic response, as described in Section 3.

In order to quantitatively evaluate the designed system's performance, several experiments were executed where the robot ran within the ground truth measurement system (GTMS), as shown in Fig. 10 [23]. The GTMS has two high-speed cameras (A504k, Basler) installed on the top right and left sides of the experimental area, which can reconstruct the spatial coordinates of the bright markers using two synchronized images captured by the cameras, running at 100 Hz. Three laser pointers were mounted on top of the main body, and the emitted red lights were projected onto the semi-transparent outer shell to form three red dots. The spatial coordinates of the three dots were reconstructed by the GTMS, and then the COM trajectories and the orientations of the main body versus time were computed from the red dots' coordinates based on the geometrical relations of the red dots to the COM.

The robot was operated to run under the GTMS using three different driving methods: only the x-axis roller actuated (Exp 1), only the y-axis roller actuated (Exp 2), and both rollers simultaneously actuated (Exp 3), each with three runs. The robot started from a resting state and moved forward about 1 m, which is the maximum range of motion the GTMS can record. In addition, another experiment was carried out to evaluate the robot's natural frequency: without any voltage input, the robot was disturbed from its equilibrium (i.e., with the initial condition $\theta_b \neq 0$), and the robot wobbled like a wobbly man. Fig. 11 shows the trajectories of the robot's geometrical center (i.e., center of the outer shell). Ideally, the robot should move along in a straight line and the main body should keep its orientation unchanged, but empirically, the robot should have motion deviations owing to the various imperfect settings in which real robots operate. Table 2 lists the root mean squared (RMS) tracking error in the lateral direction and the RMS error in the yaw orientation. Along with a 1-meter path, the lateral error is no larger than 4.1 cm. The yaw state is not controllable, as mentioned in Section 2, and on average, the main body has no more than a 13-degree deviation. Note that in ordinary operation, the direction of the robot's explicit motion can be adjusted by setting the correct ratio of input voltages for the robot. In the test reported above, no adjustments to the roller motion were executed in the middle, to act as the baseline and performance characterization. The error reported in Table 2 mainly results from two facts. First, the COM of *OmniQiu* is not perfectly located at the center. When the robot started moving, gravity created unwanted moments to the robot, so the robot's forward motion was deviated toward another direction. The other issue is friction. The contacts between all surfaces (i.e., the roller, the driven ball, the outer shell, and the ground) are basically point contacts, and it may not be sufficient to provide enough friction to reject the torque disturbance about the vertical axis, so the main body may exhibit unwanted yaw motion.

Fig. 12 shows the oscillating frequency of the main body θ_b when the robot was operated according to the different input methods described in the previous paragraph. The figure reveals that oscillations existed in all experiments and the frequency of θ_b is quite uniform, which is consistent with the simulation results reported in Section 3. We observed that in Exps 1–3 the driven ball reached its steady-state angular velocity, $\dot{\theta}_d$, within a short time period. Because the rotation of the driven ball, the outer shell, and the main body are coupled, as shown in Eq. (3), the oscillation of θ_b would result in the oscillation of θ_s when the robot was in

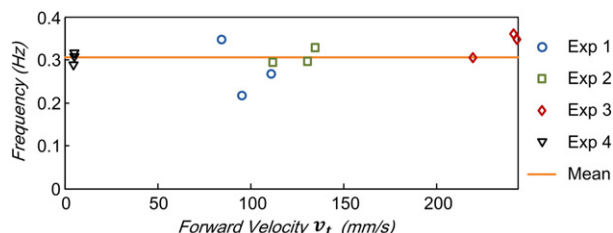


Fig. 12. Oscillating frequency of the main body when the robot was operated at different forward speeds.

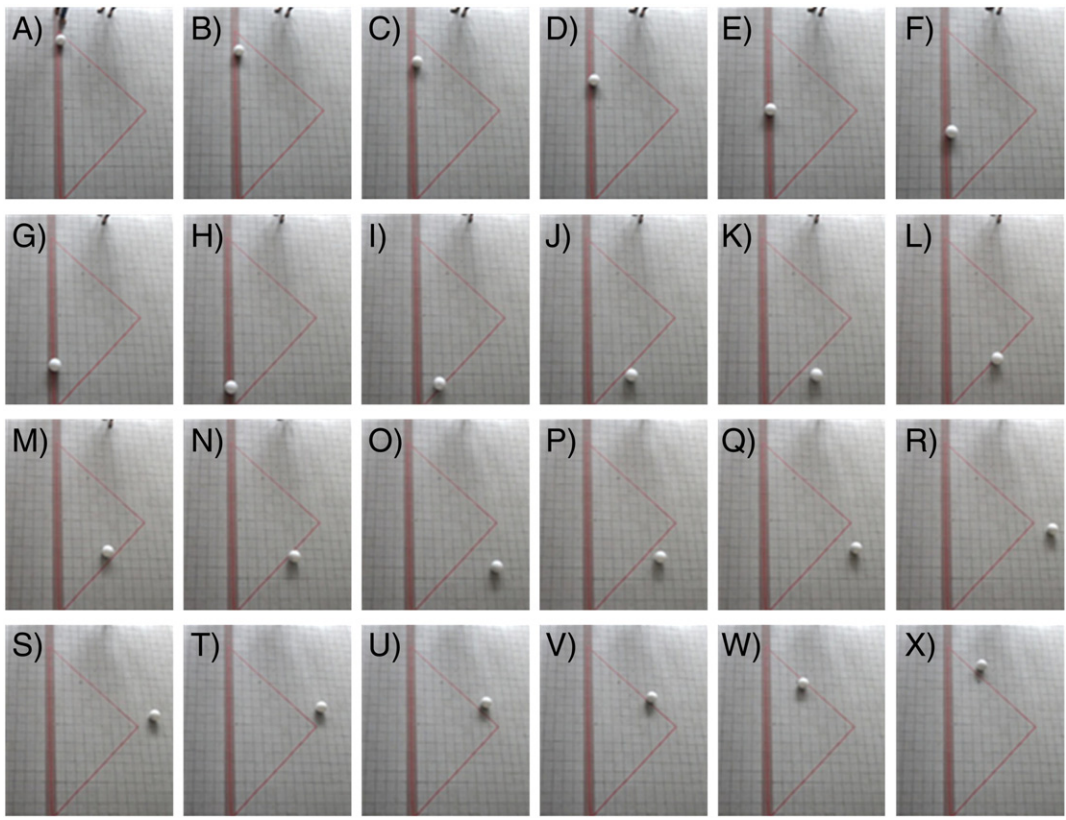


Fig. 13. The snapshots of the robot moving along a triangle route.

motion. Fig. 12 also reveals that the averaged forward velocities in Exp 1 (x-axis roller actuated) and Exp 2 (y-axis roller actuated) are not the same, but instead they are 25% different (i.e., averaged 97 mm/s in Exp 1 and 126 mm/s in Exp 2), resulting from the inconsistent empirical settings between the two axes, such as the friction condition, the gearbox efficiency, the contact surface characteristics, etc. It is worth pointing out that in Exp 3, where the robot was simultaneously driven by both rollers, the average forward velocity (235 mm/s) was faster than the resultant velocity formed by Exp 1 and Exp 2 where the robot was driven by one roller. This indicates that the overall amount of energy consumption for wearing out or other loss in Exp 3 is less than the summation of that in Exp 1 and Exp 2. Thus, when both rollers were actuated, the operating points of the motors shifted to new locations with higher speeds and lower torques. As a result, the forward velocity in Exp 3 was much larger than that of Exp 1 and Exp 2 multiplied by the squared root of 2.

In order to test the ability to perform omni-directional locomotion, the triangle route test was carried out. In the triangle route test, the robot was operated to follow an isosceles triangle with a hypotenuse of 3.8 m as shown in Fig. 13, where the size of the tile on the ground was 20 cm × 20 cm. The images of Fig. 13 are snapshots of a video that recorded the overall robot locomotion from the ceiling by a commercial digital camcorder (HDR-XR350, SONY). The time difference between two consecutive images is 3 s, and the overall motion takes 72 s. As a result, the empirical turning trajectory appeared in an arc rather than a sharp angle owing to the robot's existing momentum in the original direction. In this case, the overall momentum of the robot was altered gradually by the motor torques, and the robot motion during the turning transition was the composition of momentum decay along with the original direction and the momentum increase along with the new direction. Therefore, owing to Newton dynamics, the empirical trajectory has a larger discrepancy from the original naive trajectory with sharp turns. The phenomenon is consistent with general impressions regarding the effect of inertia. Lighter systems can have faster responses. In summary, the overall result reveals that the robot can be operated to follow the desired trajectory quite well, and omnidirectional motion is indeed achievable.

A brief discussion of mobility of the robot on the uneven terrain is listed here. Because the power of the motors used in the current implementation is very small (3 W), we found that the robot can only climb a slope with a very small incline. In addition, if it encounters a small obstacle, we have found through empirical testing that the spherical robot is almost always detoured and does not cross over the obstacle. This behavior is expected and can be roughly explained by physical phenomenon (i.e., a change of boundary condition). Normally, the spherical robot has contact with the ground with only one point; when the robot meets an obstacle, another contact point is then established. When this happens, the robot's locomotion is somewhere between (1) rotating with respect to the direction formed by two contact points and (2) opting for the path with the least increase of potential energy. The quantitative trajectory of the robot would be determined by its initial body state as well as the relative position of the added contact point to the robot. If there is a step obstacle in its way, in general, the spherical robot will

demonstrate a similar crossing behavior to that of wheeled robots because the cross-section model of both systems is the same. In general, when comparing the robots to other shapes, the spherical robot may be more easily detoured, but it rarely gets stuck because of its unique outer shape. As long as the robot has internal navigation capability, the detoured path can be recovered.

6. Conclusion

We report on the design and implementation of the novel omnidirectional spherical robot *OmniQiu*. For this robot, a smaller ball is placed inside the spherical shell and driven by two orthogonally-mounted and independently-operated rollers. The ball can be rolled in any direction due to the linear composition of the rolling forces from the rollers, thus moving the whole system. With two actuators, the robot can perform 2 DOFs of omnidirectional locomotion without any singularity configuration. A simplified planar model is constructed using the Lagrangian method to investigate the dynamics of the robot. Simulation results reveal that the forward velocity of the robot is roughly proportional to the input voltage of the motors. Owing to the outer shell's circular profile and rolling motion of the driven ball inside the outer shell, when the input voltage is applied to the robot for locomotion, the robot's main body oscillates like a pendulum. The single input of voltage affects both the rotational motion of the main body and translational motion of the outer shell (or the robot). The yaw rotation of the main body is not controllable, but this is a minor issue since this does not affect the robot's explicit translational locomotion behavior if the motion of the two rollers is adjusted. The simulation results also reveal that the components inside the shell should be placed as low as possible to increase the system's dynamic response, which was taken into consideration when designing the robot. Since the rolling behavior of the robot requires frictional force, several design considerations (such as spring mechanisms) are reported to solve this issue. The robot is built, and several experiments are conducted to evaluate its performance. The dynamic characteristics of the empirical robot (such as the main body's oscillation) match the simulation results. The lateral deviation of the robot when it is operated in forward motion is no larger than 0.041 m in a 1-meter motion course. The experimental evaluation confirms that the design concept is feasible and realistic, and the robot can be operated to follow a straight line or move along a triangular route.

Acknowledgments

This work is supported by the National Science Council (NSC), Taiwan, under contracts NSC 99-2815-C-002-077-E and 100-2628-E-002-021-MY3.

References

- [1] R.H. Armour, J.F.V. Vincent, Rolling in nature and robotics: a review, *Journal of Bionic Engineering* 3 (2006) 195–208.
- [2] A. Halme, T. Schönberg, Y. Wang, Motion control of a spherical mobile robot, *Proceedings, 4th International Workshop on Advanced Motion Control (AMC '96-MIE)*, vol. 1, 1996, pp. 259–264.
- [3] Q. Zhan, Y. Cai, C. Yan, Design, Analysis and Experiments of an Omni-Directional Spherical Robot, Presented at the IEEE International Conference on Robotics and Automation, Shanghai International Conference Center, Shanghai, China, 2011.
- [4] A. Cicchi, A. Balluchi, D. Prattichizzo, A. Gorelli, Introducing the "SPHERICLE": an experimental testbed for research and teaching in nonholonomy, *Proceedings, IEEE International Conference on Robotics and Automation (ICRA)*, vol. 3, 1997, pp. 2620–2625.
- [5] J. Alves, J. Dias, Design and control of a spherical mobile robot, *Proceedings of the Institution of Mechanical Engineers Part I-Journal of Systems and Control Engineering* 217 (2003) 457–467.
- [6] F. Michaud, S. Caron, Roball, the rolling robot, *Autonomous Robots* 12 (2002) 211–222.
- [7] M. Kabala, M. Wnuk, Design and Construction of RoBall, a Spherical, Nonholonomic Mobile Robot, 2004.
- [8] Y. Ming, D. Zongquan, Y. Xinyi, Y. Weizhen, Introducing HIT spherical robot: dynamic modeling and analysis based on decoupled subsystem, *IEEE International Conference on Robotics and Biomimetics (ROBIO)*, 2006, pp. 181–186.
- [9] D. Liu, H. Sun, Q. Jia, A family of spherical mobile robot: driving ahead motion control by feedback linearization, *2nd International Symposium on Systems and Control in Aerospace and Astronautics (ISSCAA)*, 2008, pp. 1–6.
- [10] D. Liu, H. Sun, Q. Jia, L. Wang, Motion control of a spherical mobile robot by feedback linearization, *7th World Congress on Intelligent Control and Automation (WCICA)*, 2008, pp. 965–970.
- [11] D. Liu, H. Sun, Nonlinear sliding-mode control for motion of a spherical robot, *Control Conference (CCC), 2010 29th Chinese*, 2010, pp. 3244–3249.
- [12] A. Ghanbari, S. Mahboubi, M.M.S. Fakhrabadi, Design, dynamic modeling and simulation of a spherical mobile robot with a novel motion mechanism, *IEEE/ASME International Conference on Mechatronics and Embedded Systems and Applications (MESA)*, 2010, pp. 434–439.
- [13] J.-C. Yoon, S.-S. Ahn, Y.-J. Lee, "Spherical Robot with New Type of Two-Pendulum Driving Mechanism," Presented at the 15th International Conference on Intelligent Engineering Systems, Poprad, Slovakia, 2011.
- [14] R. Mukherjee, M.A. Minor, J.T. Pukrushpan, Simple motion planning strategies for spherobot: a spherical mobile robot, *Proceedings of the 38th IEEE Conference on Decision and Control*, vol. 3, 1999, pp. 2132–2137.
- [15] A.H.J.A. P. Mojabi, Introducing August: a novel strategy for an omnidirectional spherical rolling robot, *Proceedings., IEEE International Conference on Robotics and Automation (ICRA)*, vol. 4, 2002, pp. 3527–3533.
- [16] A.H.J.A. P. Mojabi, Introducing Glory: a novel strategy for an omnidirectional spherical rolling robot, *Journal of Dynamic Systems, Measurement, and Control* 126 (2004) 678.
- [17] S. Bhattacharya, S.K. Agrawal, Spherical rolling robot: a design and motion planning studies, *IEEE Transactions on Robotics and Automation* 16 (2000) 835–839.
- [18] V.A. Joshi, R.N. Banavar, R. Hippalgaonkar, "Design, Modeling and Controllability of a Spherical Mobile Robot," Presented at the National Conference on Mechanisms and Machines, Bangalore, India, 2007.
- [19] V.A. Joshi, R.N. Banavar, R. Hippalgaonkar, Design and analysis of a spherical mobile robot, *Mechanism and Machine Theory* 45 (2010) 130–136.
- [20] Q. Jia, Y. Zheng, H. Sun, H. Cao, H. Li, Motion control of a novel spherical robot equipped with a flywheel, *International Conference on Information and Automation (ICIA)*, 2009, pp. 893–898.
- [21] G.C. Schroll, "Design of a Spherical Vehicle with Flywheel Momentum Storage for High Torque Capabilities," Bachelor Of Science, Massachusetts Institute of Technology, Massachusetts Institute of Technology, 2008.
- [22] R. Siegwart, I.R. Nourbakhsh, *Introduction to Autonomous Mobile Robots*, The MIT Press, 2004.
- [23] Y.-C. Chou, W.-S. Yu, K.-J. Huang, P.-C. Lin, Bio-inspired step-climbing in a hexapod robot, *Bioinspiration & Biomimetics* 7 (2012) 036008.